Author(s): Ylikorpi, Tomi & Forsman, Pekka & Halme, Aarne

Title: Gyroscopic Precession In Motion Modelling Of Ball-Shaped Robots

Year: 2014

Version: Post print

Please cite the original version:

Ylikorpi, Tomi & Forsman, Pekka & Halme, Aarne. 2014. Gyroscopic Precession In Motion Modelling Of Ball-Shaped Robots. Proceedings of the 28th European Conference on Modelling and Simulation. ISBN 978-0-9564944-9-8 (electronic). ISBN 978-0-9564944-8-1 (printed). DOI: 10.7148/2014-0401.

GYROSCOPIC PRECESSION IN MOTION MODELLING OF BALL-SHAPED ROBOTS

Tomi Ylikorpi
Pekka Forsman
Aarne Halme
Department of Electrical Engineering and Automation
Aalto University
P.O. Box 15500, 00076 Aalto, Finland
E-mail: tomi.ylikorpi@aalto.fi

KEYWORDS

Modelling and simulation in robotic applications, ball-shaped robots, robot dynamics, multi-body simulation

ABSTRACT

This study discusses kinematic and dynamic precession models for a rolling ball with a finite contact area and a point contact respectively. In literature, both conventions have been applied. In this paper, we discuss in detail the kinematic and dynamic models to describe the ball precession and the radius of a circular rolling path. The kinematic model can be used if the contact area and friction coefficient are sufficient to prevent slippage. The dynamic precession model has significance in multi-body simulation environments handling rolling balls with ideal point contacts. We have applied both the kinematic and dynamic precession model to evaluate the no-slip condition of the existing GimBall-robot. According to the result, the necessity of an external precession torque may cause slipping at lower velocities than expected if ignoring this torque.

SYMBOLS

d	Contact area diameter (m)
I_0	Main moment of inertia about rolling axis (kg·m^2)
I	Two other main moments of inertia (kg·m^2)
I_{pz}	Pendulum inertia about vertical axis (kg·m^2)
M_ζ	Forward rolling torque (N·m)
M_ξ	Sideways roll torque (N·m)
M_η	Torque around η-axis (N·m)
r	Path radius (m)
r_c	Path radius, to contact area center (m)
R	Ball radius (m)
R'	Effective rolling radius (m)
t	Time (s)
T_z	Torque around ground vertical Z-axis (N·m)
γ	Forward rolling angle of the ball, pitch angle (rad)
ζ	Forward rolling axis of the ball
ξ	Sideways roll axis of the ball
η	Axis orthogonal to ζ and ξ.
θ	Sideways roll angle of the ball, lean angle (rad)
$\dot{\theta}$	Sideways roll rate (rad/s)
$\ddot{\theta}$	Sideways roll acceleration (rad/s^2)
φ	Heading angle of the ball, yaw angle (rad)
Ω , $\dot{\varphi}$	Precession rate, spin rate (rad/s)
$\ddot{\varphi}$	Precession acceleration of the ball (rad/s^2)
ω	Forward rolling rate of the ball (rad/s)
$\dot{\omega}$	Forward rolling acceleration (rad/s^2)
μ	Friction coefficient at contact
μ_a	Friction coefficient share for acceleration force
μ_T	Friction coefficient share for vertical torque

INTRODUCTION

Ball-shaped vehicles have been under development already over the last 120 years. The first patents on self-propelled spherical toys were filed in the end of 19th century. Studies on dynamic modelling and steering of a motor-driven ball started in 1990's leading into emergence of computer controlled spherical mobile robots. (Ylikorpi and Suomela 2007) Recent studies on ball-shaped robots have described a variety of applications in different environments, including marine, indoors, outdoors and planetary exploration. (Michaud and Caron 2002; Bruhn et al. 2005; Kaznov and Seeman 2010) Lately, commercial spherical robots have been introduced to the markets for surveillance and gaming applications. (Avery 2011; Krieger 2013)

Spherical rolling robots offer interesting modelling and control problems due to their extraordinary dynamic nature. In development of robot mechanics and control, simulators regularly represent the robotic system and its behavior. (For example: Hristu-Varsakelis 2001; Otani et al. 2006; Jia et al. 2008; Liu et al. 2008; Ghanbari et al. 2010; Ishikawa et al. 2010; Sang et al. 2011; Zheng et al. 2011; Cai et al. 2012)

Figure 1 presents the pendulum-driven GimBall-robot developed at Aalto University. Steering of this robot takes place by tilting the rolling axis sideways with the aid of the pendulum. As shown in Figure 2, the ball then adopts a circular rolling path. The path center appears to be located at the crossing point of the tilted rolling axis extension and the rolling plane.

Although this behavior appears trivial at the first glance, several questions can be formulated:

1. What makes the ball to follow a circular path?
2. Is the path center actually located at the extension of the rolling axis? If so, why?

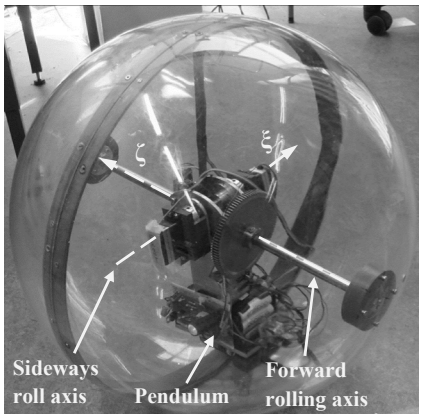

Figure 1: The *GimBall* -robot in Aalto University

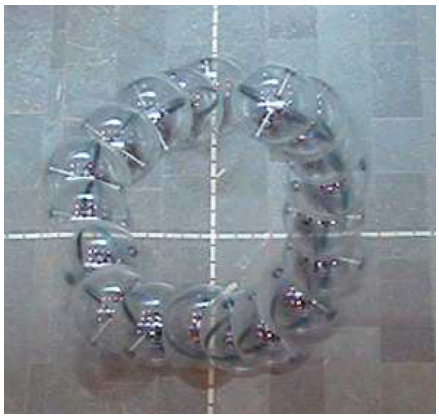

Figure 2: GimBall Follows a Circular Trajectory. Adopted from Nagai (2008)

3. Assuming no slipping or sliding, can the behavior be explained purely by geometry?
4. When the ball velocity changes, a torque around a vertical axis is needed to change the angular precession-rate. Where this torque comes from?
5. In particular, how behaves an ideal ball on an ideal plane with an ideal point contact? This is a relevant question for simulation models.
6. How do these findings reflect into practice?

This study seeks for answers for the above set questions. In particular, we are looking for the relationship between the lean angle and the path radius. The results find significance in formulation of accurate dynamic models for ball robots, and in application of those models for simulation purposes.

For our robot, forward rolling takes place around an axis whose sideways lean angle with respect to the rolling plane is assumed stable and under control. Forward and backward rolling is unlimited but sideways motion limits to the adjustment of the sideways lean angle only. Steering of the rolling direction to the right or left requires a precession motion of the rolling axis (and the entire robot) around the vertical axis. Omni-directional rolling, that can take place around any axis at any moment, is not possible for this kind of pendulum-driven robots.

RELATED WORK

Literature presents basically two different models for ball precession: it is described either as a kinematic behavior or as a dynamic one. The convention selected in the literature follows in general the mechanical design of the robot being discussed. It is in our interest to find out, whether the kinematic or a dynamic model should be used for a pendulum-driven robot, and under which circumstances is the selection valid. This section gives an overview on the ball precession models in the literature. The discussion is divided into five subsections, each considering a specific approach.

Classical ball-plate problem, spinning forbidden

Prior studies considering the rolling contact between two rigid bodies with curved surfaces lay ground for further path planning and control of rolling balls. One subset of the rolling body problem is a sphere rolling along a plane. In this set-up, the ball moves along a planar surface through rotations around horizontal axes. This is known as the *'classical ball-plate problem'*.

In the classical ball-plate problem, any rotation of the ball around the vertical axis is usually forbidden. In some cases, the ball rotates between two horizontal plates: The upper plate moves in horizontal direction, thus providing the actuation for the ball. Since the ball has no actuation of its own, especially no actuation around the vertical axis, it is practical to set the vertical rotation rate (called often *spinning*) zero. In the related literature, the complete formulae include also the spinning motion, while several examples in the same references assume no-spinning for convenience. (Cai and Roth 1987; Montana 1988; Li and Canny 1990; Jurdjevic 1993; Bicchi et al. 1995). Jurdjevic writes '*It is convenient to assume that* $\omega_3 = 0$.' On this basis, the *no-slip –constraint* is often defined as rolling without slipping, but also setting the spinning rate zero.

Some robot designs are able to rotate in any direction. Therefore, these *omni-directional ball robots* do not require vertical precession for steering. In modelling of these robots, it is beneficial to assume that the contact geometry and friction prevent spinning. (Halme et al. 1996; Bicchi et al. 1997; Spitzmüller 1998; Camicia et al. 2000; Alves and Dias 2003; Chen et al. 2012) For their omni-directional robot and based on no-spin –condition, Zhan et al. (2011) set total vertical rotation rate as zero. From the rolling velocity, lean angle and no-spin constraint they solve the ZYX-Euler rotation velocities. The result particularly describes the no-spin condition: the ball does not rotate around the vertical axis, but it rotates only around a horizontal axis.

Mukherjee et al. (1999, 2002) and Das and Mukherjee (2004, 2006) study the application of the classical ball-plate problem for path planning and steering of a ball robot. In addition, they introduce a model of a ball with a tilted rolling axis. The no-slip constraint is set effective including the no-spinning condition. Das

writes: *'The assumption $\omega_z^1 = 0$ is made in conformity with the physical constraint that the sphere cannot spin about the vertical axis.'* The ball orientation is then expressed using the body-fixed ZYZ-Euler angles. The three Euler rotation velocities are calculated to satisfy the no-spin constraint. The resulting non-zero first Euler rotation around the vertical axis is then used to describe the change-rate of ball heading.

Also Svinin and Hosoe (2006, 2008) combine the classical ball-plate problem with ball rotation around a tilted rolling axis. Assuming that the rolling axis passes through the path center, they define the path radius of the tilted ball from geometry, without referring to the no-spin constraint.

Classical ball-plate problem, free spinning

In contrast to the no-spinning constraint, most of the papers introducing momentum wheels for robot actuation leave spinning free. The no-slip condition is then defined as a pure rolling, leaving the vertical precession unconstrained. (Bhattacharya and Agrawal 2000a, 2000b; Otani et al. 2006; Ishikawa et al. 2010, 2011; Sang et al. 2011; Svinin et al. 2012a, 2012b; Morinaga et al. 2012; Azizi and Naderi 2013) Svinin relates the spinning motion to the system actuation: *''Note that we do not impose the no-spinning constraint ($\omega_z = 0$) because whether or not the system admits the pure rolling motion depends on how it is actuated.'* Ishikawa, in turn, rejects the no-spin constraint completely: '*In most of the past works concerning the rolling sphere problem, there imposed an additional assumption that the sphere never 'spins' about the vertical axis passing through the contact point. However, this assumption is no more than a technical one and is not reasonable from physical point of view.*' Hristu-Varsakelis (2001) fortifies this statement in his original work studying the dynamic case of a spinning sphere between two plates.

Joshi et al. (2007, 2010) and Joshi and Banavar (2009) give an extensive discussion on a spherical robot driven by four momentum wheels. In particular, Joshi and Banavar (p. 346-347, Figure 3) give an impression of a robot rolling around a tilted axis but following a straight path. This behavior rejects the idea of a kinematic precession model.

Yet utilizing the gyroscopic effect for stabilization and steering, another type of a robot is the rolling wheel called *Gyrover*. The Gyrover steers by tilting sideways, and the precession rate develops from the wheel dynamics without a kinematic constraint. (Brown Jr. and Xu 1996; Xu et al. 1998; Nandy and Xu 1998)

Spinning is free from constraints also in the robot models applying linear actuators in the works of Javadi and Mojabi (2002, 2004), and Sang et al. (2010).

Pendulum-driven ball robots, no-spinning constraint

To calculate the precession velocity, some papers set the no-spin constraint also for a pendulum-driven robot. In a similar manner as do Mukherjee et al. (2002), they solve the first Euler rotation velocity around the vertical axis, and use it as precession rate. (Zheng et al. 2011; Cai et al. 2012)

Pendulum-driven ball robots, kinematic precession model

Many studies define the path curvature directly from the ball radius and the sideways lean angle. (Laplante et al. 2007; Nagai 2008; Liu et al. 2008; Liu and Sun 2010; Ghanbari et al. 2010; Mahboubi et al. 2013) Kim et al. (2009) start their study with a description of a finite contact area between a ball and a plane. The case is similar to that of a conical roller. They then extend the kinematic constraint to apply also for a point contact. Ball precession is kinematically constrained also in the work of Kamaldar et al. (2011).

Pendulum-driven ball robots, dynamic precession model

Literature presents one dynamic model giving the ball precession rate through torque balance between the gravitational torque, the centrifugal torque, and the gyroscopic torque. The result gives the precession rate as a function of the pendulum angle and the rolling rate, but ignores the sideways lean angle. (Nagai 2008; Kayacan et al. 2012). Also Jia et al. (2008) leave the ball precession free from kinematic constraints.

ROLLING PATH RADIUS WITH A FINITE CONTACT AREA

In quest for an answer for our first question "What makes the ball to follow a circular path?" –we start our study with a view on a ball with a finite contact area.

Figure 3 presents a ball with a finite contact area. A spherical shell with a finite stiffness adopts a circular contact area with a finite diameter d. Then, under no-slip conditions, the contact geometry defines the ball motion to be similar to that of a conical roller. The figure shows the illustrative cone inside the ball. A non-zero vertical torque T_z indicates that contact friction over a finite contact area is able to exert a vertical torque on the ball.

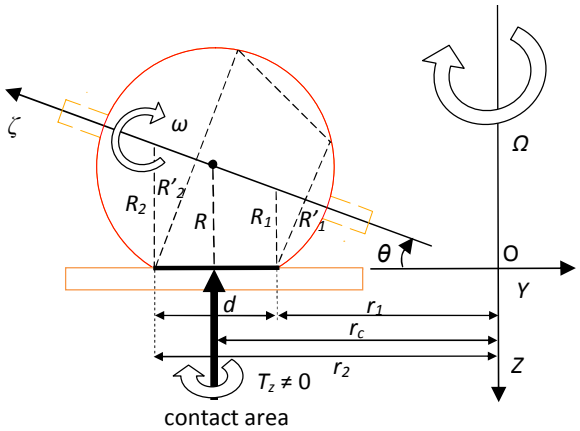

Figure 3: A Rolling Ball with a Finite Contact Area

The following calculations –based on the contact kinematics, solve the path radius, the center of the circular path, and the precession velocity. Note that in Figure 3, the circular path center O is not yet fixed with respect to the ball. The path center location becomes known only after the radiuses r_1 and r_2 are solved.

Under no-slip –conditions, the roller velocity at any contact point is zero. Equation (1) presents the kinematic condition at the extreme points of the contact area.

$$\begin{cases} -\omega R'_1 + \Omega r_1 = 0 \\ -\omega R'_2 + \Omega r_2 = 0 \end{cases} \quad (1)$$

Notifying the roller geometry, (1) is identical with

$$\begin{cases} \omega R_1 \cos\theta = \Omega r_1 \\ \omega \underbrace{(R_1 \cos\theta + d\sin\theta)}_{R_2} = \Omega \underbrace{(r_1 + d)}_{r_2}. \end{cases} \quad (2)$$

In this kinematically constrained situation, the precession rate Ω can be solved from (2) as a function of the rolling rate ω and the lean angle θ.

$$\Omega = \omega \sin\theta \quad (3)$$

Substituting (3) into (2) gives the velocity-independent kinematic equations (4) for solving the path radius.

$$\begin{cases} \omega R_1 \cos\theta = \omega \sin\theta\, r_1 \\ \omega R_2 \cos\theta = \omega \sin\theta\, r_2 \end{cases} \quad (4)$$

Equation (4) can be expressed as

$$\frac{R_1}{r_1} = \frac{R_2}{r_2} = \tan\theta. \quad (5)$$

Equation (5) applies to all points on the contact area. As r_c presents the path radius measured to the center of the contact area, (5) can be written as

$$r_c = \frac{R}{\tan\theta}. \quad (6)$$

Equation (6) indicates that the rolling axis ζ of the cone indeed passes through the path center O.

In case of a finite contact area, this result gives answers to our three first questions: In such case, the no-slip condition and contact kinematics invoke the precession motion and make the ball to follow a circular path, whose center is located at the point where the extension of the tilted rolling axis meets the rolling plane.

The next question is: Can this result be extended to apply also for a ball with a point contact? To answer to this question, we have a look at the calculations we have made: The kinematically constrained precession rate (3) was derived by solving the equation pair in (2). Re-arranging of (2) gives

$$\begin{cases} \omega R_1 \cos\theta = \Omega r_1 \\ \omega R_1 \cos\theta + \omega d\sin\theta = \Omega r_1 + \Omega d \end{cases} \quad (7)$$

$$\Leftrightarrow \begin{cases} \omega R_1 \cos\theta - \Omega r_1 = 0 \\ \omega R_1 \cos\theta - \Omega r_1 = d(\Omega - \omega\sin\theta) \end{cases}. \quad (8)$$

If the length d was zero, i.e. the contact comprises a point, (8) is equivalent with (9).

$$\Leftrightarrow \begin{cases} \omega R_1 \cos\theta - \Omega r_1 = 0 \\ 0 = 0 \end{cases}, d = 0 \quad (9)$$

The lower row of (9) is identically true and the two unknowns (path radius and precession rate) can't be solved with the one remaining equation in (9). On basis of this result, the conical roller analogy can't be extended for a point contact. The no-slip –condition still prevails, but it does not define the precession rate of the ball. Path radius of a rolling ball can then be different from what would be expected on based on the kinematic model. Such point contact could be present, for example, at the contact of a rolling disc or a rolling ideal sphere.

ROLLING PATH RADIUS DERIVED FROM BALL DYNAMICS

An ideal sphere with a point contact may be encountered for example in simulation experiments of ball-shaped robots, especially in multi-body simulation environments, like Adams. As was discovered in the previous section, in this particular case the kinematic model can't be used to define the path radius, and some other solution must be found. This section seeks to solve the precession rate from ball dynamics.

Figure 4 presents a ball with a point contact. A zero torque T_z indicates the lack of the vertical friction torque, which is due to the point contact that does not provide any moment arm for lateral friction forces. Path radius r and precession velocity Ω are unknown. The forward rolling axis ζ crosses the rolling plane at point P located at the distance of $R/\tan\theta$ from the contact point. Note that we have not placed the path center O in any specific location with respect to the ball center. Distance from the crossing point P to the path center O depends solely on the path radius r, which is yet unknown. This means also that the crossing point P on the rolling plane is not necessarily stationary.

The general rolling constraint presented in (1) remains valid and it can be expressed as in (10). Path radius r can be solved from (10) once the precession rate Ω is known.

$$\omega R' \equiv \omega R \cos\theta = \Omega r \quad (10)$$

Equations of motion for a rotating body provide the necessary tools for solving the precession rate. Equation (11) presents Euler's equations for a rotationally

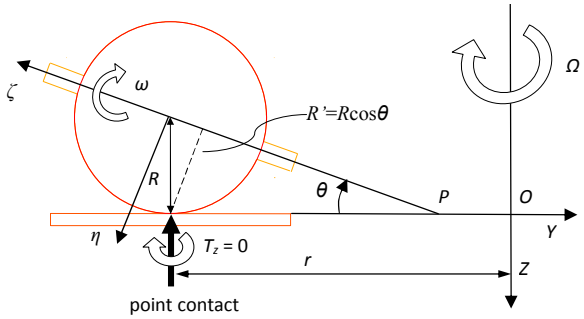

Figure 4: A Rolling Ball with a Point Contact

symmetric object, adapted from Hibbeler (2009, p. 603-615) to apply the notation of Figure 4. This particular form of Euler's equations has been modified for analysis of a spinning top. The moving frame of reference follows the nutation and precession of the top, but does not spin with it. In particular, the accelerations need to be determined in the moving frame.

$$\begin{aligned} M_\xi &= I\left(\ddot{\theta} + \Omega^2 \sin\theta\cos\theta\right) + I_0\Omega\cos\theta(-\Omega\sin\theta + \omega) \\ M_\eta &= I\left(\dot{\Omega}\cos\theta - 2\Omega\dot{\theta}\sin\theta\right) - I_0\dot{\theta}(-\Omega\sin\theta + \omega) \\ M_\zeta &= I_0\left(\dot{\omega} - \dot{\Omega}\sin\theta - \Omega\dot{\theta}\cos\theta\right) \end{aligned} \quad (11)$$

The left-hand side of (11) presents the torques affecting the ball, and the right-hand side presents its motion and inertia terms. I_0 stands for the inertia around the rolling axis ζ, and I indicates the inertia around the principal axes η and ξ. The inertias I_0 and I are not assumed to be identical, but they may differ, for example due to the mechanical structure of the robot's spherical shell. Equation (12) presents torque balance around the vertical axis.

$$M_\eta\cos\theta - M_\zeta\sin\theta - T_Z = 0 \quad (12)$$

Substituting (11) into (12) with consideration of ball inertia about vertical axis gives precession acceleration:

$$\dot{\Omega} = \frac{T_Z + 2\Omega\dot{\theta}\sin\theta\cos\theta(I - I_0) + I_0\left(\dot{\theta}\omega\cos\theta + \dot{\omega}\sin\theta\right)}{I\cos^2\theta + I_0\sin^2\theta + I_{pz}} \quad (13)$$

Equation (13) presents a dynamic model for the ball precession. The model includes rolling velocity and the lean angle of the robot, their time derivatives, and the two main moments of inertia.

Recall that Equations (11) and (12) represent the spherical shell alone neglecting any other parts of the robot. For completeness, the denominator of (13) has been added with the driving mechanism inertia I_{pz} around the ground vertical. Exact pendulum angle and inertia I_{pz} are functions of ball precession velocity, lean angle and path radius. For brevity, a theoretical scalar-valued maximum inertia of the pendulum presents a worst-case estimate for I_{pz}. In the following, the simulation results are repeated with and without the pendulum inertia. We may also note that in absence of pendulum inertia, the model in (13) is general for rolling spheres and applicable for many different types of ball-robots. Only requirement is that the shell rotates around a tilted rolling axis. This model can then be completed with the specific inertial properties of the robot being under investigation.

For demonstration purposes, the model in (13) can be simplified to present an ideally controlled ball having a constant lean angle θ. In case of a constant lean angle, the precession acceleration becomes

$$\dot{\Omega} = \frac{T_z + I_0\dot{\omega}\sin\theta}{I\cos^2\theta + I_0\sin^2\theta + I_{pz}}, \dot{\theta} = 0 \quad (14)$$

The precession acceleration is now a function of the ball rolling acceleration. In absence of external torque and during a steady-state rolling, precession rate remains constant and the ball follows a steady circular path. Upon ball acceleration, precession rate develops respectively and the ball maintains the same circular path. During acceleration from rest to the final rolling velocity ω, the ball precession velocity Ω can be acquired through integration of (14). In absence of external torque and assuming a constant worst-case I_{pz}

$$\Omega = \frac{I_0\omega\sin\theta}{I\cos^2\theta + I_0\sin^2\theta + I_{pz}}, T_z = 0 \quad (15)$$

The path radius can then be solved from (10) and (15)

$$\omega R\cos\theta = \frac{I_0\omega\sin\theta}{I\cos^2\theta + I_0\sin^2\theta + I_{pz}} \cdot r, \quad (16)$$

$$\Leftrightarrow r = \left(\frac{I}{I_0}\cos^2\theta + \sin^2\theta + \frac{I_{pz}}{I_0}\right)\cdot\frac{R}{\tan\theta}. \quad (17)$$

Equation (17) presents the path radius for a ball that maintains a constant lean angle, being independent from ball velocity or acceleration. It is interesting to note that in case of a uniform sphere without any pendulum, $I = I_0$, $I_{pz} = 0$ and (17) is equivalent with (6), and (15) equals to (3). This means that, under no-slip conditions, the dynamic behavior of a uniform ball with a point contact is similar to the kinematic behavior of a ball with a finite contact area. In general and due to differences in main moments of inertia, this is not the case. For a constant lean angle, comparison of the path radius from the dynamic model (17) with the kinematic model (6) reveals the ratio

$$r_{kinematic}/r_{dynamic} = \left(\frac{I}{I_0}\cos^2\theta + \sin^2\theta + \frac{I_{pz}}{I_0}\right) \quad (18)$$

In practical applications, the robot's main moment of inertia I_0 around the forward rolling axis is often smaller than the inertia I about the two other axes. As a practical example, the GimBall-robot robot shell in Figure 1 has the inertia ratio 1.18. Assuming a 0.2 rad lean angle and a point contact, the dynamic model attains a path radius 17% larger than suggested by the kinematic model. GimBall pendulum inertia may enlarge the path radius up to 41% beyond the kinematic model.

SIMULATION AND RESULTS

For simulation purposes, the precession acceleration and rate can be calculated in a closed form from (14) and (15). In this example, constant lean angle and rolling acceleration are applied for a given acceleration time T_a

$$\dot{\omega}(t) = \begin{cases} \dot{\omega} & , 0 \le t \le T_a \\ 0 & , t > T_a \end{cases}. \quad (19)$$

Equation (20) shows the resulting rolling velocity ω, and the precession acceleration comes from (14) according to (21).

$$\omega(t) = \begin{cases} t\dot{\omega} & , 0 \le t \le T_a \\ T_a\dot{\omega} & , t > T_a \end{cases} \quad (20)$$

$$\dot{\Omega}(t) = \begin{cases} \frac{I_0\dot{\omega}\sin\theta}{I\cos^2\theta + I_0\sin^2\theta + I_{pz}} & , 0 \le t \le T_a \\ 0 & , t > T_a \end{cases} \quad (21)$$

Integration of (21) gives the precession velocity Ω in (22). Further integration gives the ball heading φ

according to (23).

$$\Omega(t) = \int_0^t \dot{\Omega}(t)dt = \int_0^t \frac{I_0\dot{\omega}\sin\theta}{I\cos^2\theta + I_0\sin^2\theta + I_{pz}}dt =$$

$$= \begin{cases} \frac{I_0\dot{\omega}t\sin\theta}{I\cos^2\theta + I_0\sin^2\theta + I_{pz}} & ,0 \le t \le T_a \\ \frac{I_0\dot{\omega}T_a\sin\theta}{I\cos^2\theta + I_0\sin^2\theta + I_{pz}} & ,t > T_a \end{cases} \quad (22)$$

$$\varphi(t) = \int_0^t \Omega(t)dt = \int_0^t \left(\int_0^t \frac{I_0\dot{\omega}t\sin\theta}{I\cos^2\theta + I_0\sin^2\theta + I_{pz}}dt \right) dt =$$

$$= \begin{cases} \frac{I_0\dot{\omega}t^2\sin\theta}{2\left(I\cos^2\theta + I_0\sin^2\theta + I_{pz}\right)} & ,0 \le t \le T_a \\ \frac{I_0\dot{\omega}T_a\sin\theta}{I\cos^2\theta + I_0\sin^2\theta + I_{pz}} \cdot \left(t - \frac{T_a}{2}\right) & ,t > T_a \end{cases} \quad (23)$$

Knowing the rolling velocity ω and heading φ, the ball velocity components v_x and v_y can be calculated as

$$\begin{cases} v_x = R\omega(t)\cos\theta \cdot \cos\varphi(t) \\ v_y = R\omega(t)\cos\theta \cdot \sin\varphi(t) \end{cases} \Leftrightarrow \quad (24)$$

$$v_x = \begin{cases} Rt\dot{\omega}\cos\theta\cos\left(\frac{I_0\dot{\omega}t^2\sin\theta}{2\left(I\cos^2\theta + I_0\sin^2\theta + I_{pz}\right)}\right), 0 \le t \le T_a \\ RT_a\dot{\omega}\cos\theta\cos\left(\frac{I_0\dot{\omega}T_a\sin\theta \cdot \left(t - \frac{T_a}{2}\right)}{I\cos^2\theta + I_0\sin^2\theta + I_{pz}}\right), t > T_a \end{cases}$$

$$v_y = \begin{cases} Rt\dot{\omega}\cos\theta\sin\left(\frac{I_0\dot{\omega}t^2\sin\theta}{2\left(I\cos^2\theta + I_0\sin^2\theta + I_{pz}\right)}\right), 0 \le t \le T_a \\ RT_a\dot{\omega}\cos\theta\sin\left(\frac{I_0\dot{\omega}T_a\sin\theta \cdot \left(t - \frac{T_a}{2}\right)}{I\cos^2\theta + I_0\sin^2\theta + I_{pz}}\right), t > T_a \end{cases} \quad (25)$$

An adaptive Gauss-Kronrod quadrature function, provided by Matlab software, was used to numerically integrate the ball's location from the velocities in (25), applying the default values for absolute error tolerance (1E-10) and relative error tolerance (1E-6).

Figure 5 demonstrates ball paths with varying inertia ratios, but with a constant 0.2-rad lean angle and constant 1-rad/s^2 acceleration to reach the 1-rad/s forward rolling velocity at t = 1 s. Ball radius is 0.226 m. The precession motion develops during the 1-s acceleration period after which the ball continues rolling with constant velocity and precession rate until the end of simulation at t = 100 s. Two separate results are produced with parallel simulations: one in Matlab using the equations derived above and marked with 'o', and another in Adams multi-body simulation software and marked with 'x'. The figure shows no differences in the parallel simulation results. During a 100-s simulation the ball rolled 22 m, while the maximum measured location difference between the two simulation results remains below 0.00013 mm. The difference is less than $6{\cdot}10^{-7}$ percent of the travelled distance.

As well in Figure 5, a third simulation result marked with 'Δ' was added to demonstrate the effect from the theoretical maximum GimBall pendulum inertia around the vertical axis. In this simulation, shell rolling inertia is 0.0633 kg·m^2, pendulum mass 1.795 kg, pendulum length 0.065 m and max. pendulum main moment of inertia 0.0074 kg·m^2, as derived from a 3D-model. The added 0.015 kg·m^2-pendulum inertia makes the

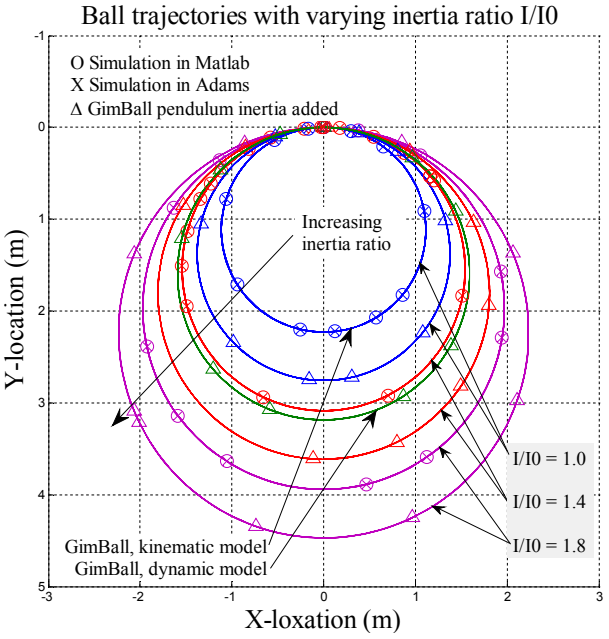

Figure 5: Ball Trajectories with Varying Inertia Ratio, with and without the Added GimBall Pendulum Inertia. Ball Radius 0.224 m, Lean Angle 0.2 rad

simulated rolling paths significantly larger.

The simulation results in Figure 5 demonstrate how different inertia ratios lead to different paths, even though the lean angle, the rolling velocity acceleration, and the final velocity are the same. This is a clear difference to the kinematic precession model. The presence of the pendulum makes the difference even larger. The innermost path in Figure 5 describes the inertia ratio 1, being similar to the result from the kinematic constraint. The difference between this path and the other paths reveals the different behavior of the dynamic and kinematic models.

COMBINING THE KINEMATIC AND DYNAMIC MODELS

We have now discovered that, with a finite contact area, a kinematic precession model can be used to define the radius of the circular path, as long as the no-slip condition prevails. We have also learned that there exists a gyroscopic torque that creates a precession motion even in absence of the kinematic rolling constraint. Now, it is of interest to study the circumstances where the kinematic rolling constraint remains valid.

The kinematic precession model requires that the contact friction provides the necessary forces to maintain (and also to change) the ball state of motion. The friction forces are needed to accelerate the ball velocity, to prevent sliding under centrifugal force, and as well to create the vertical torque to change the precession rate, if not created by the gyroscopic forces as shown in (13). Depending on the inertia ratio, gyroscopic precession torque may increase or decrease the needed external friction torque. In order to create the

sufficient torque, the contact geometry needs to have a sufficient diameter. In this section, based on the kinematic and dynamic precession models, we calculate the minimum necessary contact area diameter. With this contact area, the kinematic precession model remains valid and the ball follows the anticipated circular path.

In case of a finite contact area depicted in Figure 3, the time derivative of the kinematic equation (3) connects the ball precession rate change to the ball forward rolling acceleration

$$\dot{\Omega} = \dot{\omega} \sin\theta. \tag{26}$$

With a given lean angle θ, the dynamic equation (14) presents the precession acceleration as a function of the vertical friction torque and precession torque. The necessary friction torque can then be solved

$$T_z = \dot{\omega} \sin\theta \cdot \left[I_0 \left(\frac{I}{I_0} - 1 \right) cos^2\,\theta + I_{pz} \right] . \tag{27}$$

In (27) one may note that a symmetric ball (without a pendulum) would not need any external friction torque. In such case the gyroscopic torque on the ball creates the necessary precession acceleration. We may see also that the friction torque is needed only when the ball rolling velocity changes.

In case of the GimBall-robot, the needed external precession torque for the shell at 0.2 rad lean angle and 1 rad/s forward rolling angular acceleration is 2.17 mNm. Addition of the maximum theoretical pendulum inertia increases the torque need to 5.15 mNm.

The contact pressure is assumed to be uniform over the circular contact area. The friction force over the surface builds up of two components: a) Lateral acceleration friction force counteracts the forward acceleration and centrifugal acceleration force. This force distributes evenly over the contact area and has the same direction at every point. b) Vertical friction torque develops from lateral force components that have uniform magnitude, but direction vectors rotate around the contact point. To prevent slipping, the maximum combined friction force shall not exceed the contact friction created by the ball weight and the coefficient of friction.

Respectively with the two force components mentioned above, the contact friction coefficient is divided into two components: μ_a covers the lateral acceleration force, and μ_T covers the vertical friction torque. To prevent slipping, the total friction coefficient needed is the sum of these

$$\mu = \mu_a + \mu_T . \tag{28}$$

Friction force providing the lateral acceleration is independent from the contact area. The necessary lateral friction coefficient can be calculated from the lateral ball acceleration and the centrifugal acceleration as

$$(mg\mu_a)^2 = (mR\dot{\omega}\cos\theta)^2 + (mr\Omega^2)^2 \tag{29}$$

Since the motion follows a circular trajectory, the precession rate and path radius can be inserted from (3) and (6):

$$(mg\mu_a)^2 = (mR\dot{\omega}\cos\theta)^2 + \left(m\frac{R}{\tan\theta}(\omega\sin\theta)^2 \right)^2 \tag{30}$$

$$\Leftrightarrow (mg\mu_a)^2 = (mR\dot{\omega}\cos\theta)^2 + (mR\cos\theta\,\omega^2\sin\theta)^2 \tag{31}$$

The friction force needed for the given vertical precession torque depends on the contact area. The torque can be calculated as an integral over the contact area A

$$T_z = 4\int_0^{\frac{\pi}{2}}\int_0^{\frac{d}{2}} (\mu_T \cdot \underbrace{\frac{4mg}{\pi d^2}}_{\substack{\text{contact} \\ \text{pressure}}} \cdot \rho \cdot \underbrace{\mathrm{d}\rho \cdot \rho \mathrm{d}\alpha}_{\mathrm{d}A}) , \tag{32}$$

where m = ball mass, ρ = distance from contact area center, and α = angular location of the force element. This gives

$$\begin{aligned} T_z &= \frac{\mu_T mgd}{3} \\ \Leftrightarrow \mu_T &= \frac{3T_z}{mgd} . \end{aligned} \tag{33}$$

Equation (33) relates the vertical friction torque to the contact area diameter, normal contact force, and friction coefficient. The same model is applied in CONTACT-statement of Adams simulation software. The necessary contact diameter can be solved from (28), (31) and (33):

$$\begin{aligned} \mu &= \frac{R\sqrt{(\dot{\omega}\cos\theta)^2 + (\cos\theta\omega^2\sin\theta)^2}}{g} + \frac{3T_z}{mgd} \\ \Leftrightarrow d &= \frac{3T_z}{m\left(\mu g - R\sqrt{(\dot{\omega}\cos\theta)^2 + (\cos\theta\omega^2\sin\theta)^2}\right)} \end{aligned} \tag{34}$$

Inserting the necessary friction torque T_z from (27) to (34) gives the needed contact diameter:

$$d = \frac{3\dot{\omega}\sin\theta \cdot \left[I_0 \left(\frac{I}{I_0} - 1 \right) cos^2\,\theta + I_{pz} \right]}{m\left(\mu g - R\sqrt{(\dot{\omega}\cos\theta)^2 + (\cos\theta\omega^2\sin\theta)^2}\right)} \tag{35}$$

In (35) one may note that in a symmetric case *($I=I_0$)* and in absence of the pendulum inertia, d = 0, i.e. a symmetric ball with a point contact will satisfy the constraints. This is because the gyroscopic torque on the symmetric ball creates the necessary precession acceleration. No external contact friction torque is needed. In a non-symmetric case a non-zero contact diameter is needed.

Assuming a coefficient of friction μ = 0.2 (typical for acrylic material used for the GimBall shell), ball radius 0.226 m, GimBall mass m = 5.1 kg, inertia ratio 1.18, and I_0 = 0.0633 kg·m^2, the needed contact area diameter becomes d = 0.75 mm at the given 1-rad/s forward rolling velocity, 1-rad/s^2 angular acceleration, and 0.2-rad sideways lean angle. With the maximum theoretical pendulum inertia 0.015 kg·m^2 added, the needed contact area diameter is 1.76 mm.

Figure 6 presents the result from (35) as a function of ball velocity and friction coefficient. As the centrifugal acceleration increases along with the increased rolling velocity, the remaining friction force available for the vertical friction torque decreases. Therefore, the necessary contact area increases. As the needed contact area diameter escapes to infinity, the forward acceleration and centrifugal acceleration consume all

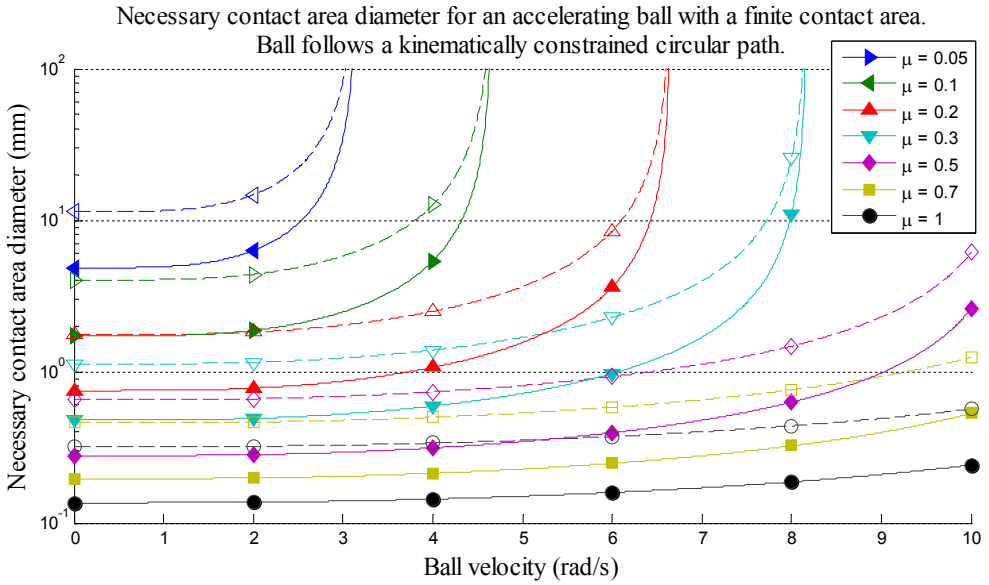

Figure 6: Necessary Contact Area Diameter for an Accelerating GimBall with Different Contact Friction Coefficients. Rolling Acceleration 1 rad/s^2, Lean Angle 0.2 rad, Path Radius 1.1 m. Dashed lines with open markers indicate the maximum effect of the GimBall pendulum inertia

available friction force capacity, and no friction torque to maintain the precession acceleration remains left. Added inertia from the elevated pendulum increases the necessary contact area. The curved graphs indicate that, due to necessary precession torque, slipping may start earlier than anticipated from rolling acceleration and centrifugal acceleration alone.

The results in Figure 6 assume that the lean angle and path radius remain constant. In addition to contact properties, the ability of the robot to follow this path depends also on the steering mechanism. In case of the GimBall-robot, the short pendulum length limits the maximum rolling velocity along this path to 1.05 m/s. Therefore, GimBall loses the track rather by flipping aside than sliding. Slippage becomes evident only at low coefficients of friction or at higher acceleration.

CONCLUSIONS

This study has discussed the kinematic and dynamic precession models for a rolling ball with a finite contact area and a point contact respectively. In literature, both conventions have been applied.

Usually, literature does not define the contact geometry. Instead, ideal spheres and planes are regularly introduced without mentioning a possibility for deformation or a finite contact area. Reader is then tempted to assume that the presented models in literature comprise a point contact. However, these models often employ the kinematic precession model, which applies for a point contact only in a case of an ideal symmetric sphere where $I=I_0$. In practical applications, such ideal symmetry can rarely be assumed.

In multi-body dynamics simulators, like Adams, the selection of the finite contact area versus a point contact makes a difference. In Adams, the GCON (general constraint) –statement can be used to create an ideal point contact. For a ball with the point contact, the dynamic precession model then prevails instead of the kinematic one. In contrast, the CONTACT –statement in Adams creates a contact with a finite contact area. In this case, the kinematic precession model applies, -as long as contact friction is sufficient. If the simulator model presents an ideal point contact but a kinematic behavior is desired, it is necessary to implement additional artificial constraints to invoke the kinematic precession model.

We have introduced the dynamic precession model for a rolling ball-robot. This model explains ball precession in presence of an ideal point contact. The absence of pendulum parameters allows application of the model for different types of ball-shaped robots. The model can be used in simulators, and it provides also information about the gyroscopic precession torque.

We have applied both the kinematic and dynamic precession model to evaluate the no-slip condition of the GimBall-robot. The result indicates that ball slipping may start earlier than anticipated if neglecting the need for an external precession torque.

In the progressive studies, the scalar-valued worst-case pendulum inertia estimate I_{pz} may be replaced with an exact presentation taking into consideration the actual pendulum orientation. Experimental tests call for robots with especially rigid spherical shells to demonstrate the effect of a minute contact area on a slippery surface.

REFERENCES

Alves, J. and Dias, J. 2003. "Design and control of a spherical mobile robot." *Proceedings Of The Institution Of Mechanical Engineers Part I-Journal of Systems and Control Engineering* 217, No.6, 457-467.

Avery, G. 2011. "Sphero rolling out as orders tumble in." *Denver Business Journal*, Dec 2, 2011, A1.

Azizi, M.R. and Naderi, D. 2013. "Dynamic modeling and trajectory planning for a mobile spherical robot with a 3Dof inner mechanism." *Mechanism and Machine Theory* 64, 251-261.

Bhattacharya, S. and Agrawal, S.K. 2000a. "Design, experiments and motion planning of a spherical rolling robot." In *Proceedings of IEEE International Conference on Robotics and Automation* (San Francisco, CA, April 2000). IEEE, 1207-1212.

Bhattacharya, S. and Agrawal, S.K. 2000b. "Spherical rolling robot: a design and motion planning studies." *IEEE Transactions on Robotics and Automation* 16, No.6, 835-839.

Bicchi, A.; Balluchi, A.; Prattichizzo, D. and Gorelli, A. 1997. "Introducing the "SPHERICLE": an experimental testbed for research and teaching in nonholonomy." In *Proceedings of IEEE International Conference on Robotics and Automation* (Albuquerque, NM, April 1997). 2620-2625.

Bicchi, A.; Prattichizzo, D. and Sastry, S.S. 1995. "Planning motions of rolling surfaces." In *Proceedings of IEEE Conference on Decision and Control* (New Orleans, Dec. 1995). 2812-2817.

Brown Jr., H.B. and Xu, Y. 1996. "A single-wheel, gyroscopically stabilized robot." In *Proceedings of IEEE International Conference on Robotics and Automation* (Minneapolis, MN, April 1996). IEEE, 3658-3663.

Bruhn, F.C.; Pauly, K. and Kaznov, V. 2005. "Extremely low mass spherical rovers for extreme environments and planetary exploration enabled with MEMS." *European Space Agency, (Special Publication) ESA SP 603*, 347-354.

Cai, C. and Roth, B. 1987. "On the spatial motion of a rigid body with point contact." In *Proceedings of IEEE International Conference on Robotics and Automation* (Raleigh, NC, Mar. 1987). IEEE, 686-695.

Cai, Y.; Zhan, Q. and Xi, X. 2012. "Path tracking control of a spherical mobile robot." *Mechanism and Machine Theory* 51, 58-73.

Camicia, C.; Conticelli, F. and Bicchi, A. 2000. "Nonholonomic kinematics and dynamics of the Sphericle." In *Proceedings of IEEE/RSJ International Conference on Intelligent Robots and Systems* (Takamatsu, Japan, Nov. 2000). 805-810.

Chen, W.; Chen, C.; Yu, W.; Lin, C. and Lin, P. 2012. "Design and implementation of an omnidirectional spherical robot Omnicron." In *Proceedings of IEEE/ASME International Conference on Advanced Intelligent Mechatronics* (Kachsiung, July 2012). IEEE, 719-724.

Das, T. and Mukherjee, R. 2004. "Exponential stabilization of the rolling sphere." *Automatica* 40, No.11, 1877-1889.

Das, T. and Mukherjee, R. 2006. "Reconfiguration of a rolling sphere: A problem in evolute-involute geometry." *ASME Journal of Applied Mechanics* 73, No.4, 590-597.

Ghanbari, A.; Mahboubi, S. and Fakhrabadi, M.M.S. 2010. "Design, dynamic modeling and simulation of a spherical mobile robot with a novel motion mechanism." In *Proceedings of IEEE/ASME International Conference on Mechatronic and Embedded Systems and Applications* (Qingdao, Shan Dong, July 2010). 434-439.

Halme, A.; Schonberg, T. and Wang, Y. 1996. "Motion control of a spherical mobile robot." In *Proceedings of IEEE International Workshop on Advanced Motion Control* (Mie, 18-21 Mar.). 259-264.

Hibbeler, R.C. 2009. *Engineering Mechanics: Combined Statics & Dynamics.* 12th ed. Prentice Hall, Upper Saddle River, NJ.

Hristu-Varsakelis, D. 2001. "The dynamics of a forced sphere-plate mechanical system." *IEEE Transactions on Automatic Control* 46, No.5, 678-686.

Ishikawa, M.; Kitayoshi, R. and Sugie, T. 2010. "Dynamic rolling locomotion by spherical mobile robots considering its generalized momentum." In *Proceedings of Society of Instrument and Control Engineers Annual Conference* (Taipei, Aug. 18-21). IEEE, 2311-2316.

Ishikawa, M.; Kitayoshi, R. and Sugie, T. 2011. "Volvot : A spherical mobile robot with eccentric twin rotors." In *Proceedings of IEEE International Conference on Robotics and Biomimetics* (Karon Beach, Phuket, Dec. 2011). IEEE, 1462-1467.

Javadi, A.H.A. and Mojabi, P. 2002. "Introducing August: a novel strategy for an omnidirectional spherical rolling robot." In *Proceedings of IEEE International Conference on Robotics and Automation* (Washington, DC, May 2002). IEEE, 3527-3533.

Javadi, A.H.A. and Mojabi, P. 2004. "Introducing Glory: A novel strategy for an omnidirectional spherical rolling robot." *Journal of Dynamic Systems, Measurement and Control, Transactions of the ASME* 126, No.3, 678-683.

Jia, Q.; Sun, H. and Liu, D. 2008. "Analysis of Actuation for a Spherical Robot." In *Proceedings of IEEE Conference on Robotics, Automation and Mechatronics* (Chengdu, China, 21-24 Sept.). 266-271.

Joshi, V.A. and Banavar, R.N. 2009. "Motion analysis of a spherical mobile robot." *Robotica* 27, No.3, 343-353.

Joshi, V.A.; Banavar, R.N. and Hippalgaonkar, R. 2007. "Design, modeling and controllability of a spherical mobile robot." In *Proceedings of National Conference on Mechanisms and Machines* (Bangalore, India, Dec. 2007). 135-140.

Joshi, V.A.; Banavar, R.N. and Hippalgaonkar, R. 2010. "Design and analysis of a spherical mobile robot." *Mechanism and Machine Theory* 45, No.2, 130-136.

Jurdjevic, V. 1993. "The geometry of the plate-ball problem." *Archive for Rational Mechanics and Analysis* 124, No.4, 305-328.

Kamaldar, M.; Mahjoob, M.J.; Haeri Yazdi, M.; Vahid-Alizadeh, H. and Ahmadizadeh, S. 2011. "A control synthesis for reducing lateral oscillations of a spherical robot." In *Proceedings of IEEE International Conference on Mechatronics* (Istanbul, Apr. 2011). 546-551.

Kayacan, E.; Bayraktaroglu, Z.Y. and Saeys, W. 2012. "Modeling and control of a spherical rolling robot: a decoupled dynamics approach." *Robotica* 30, No.4, 671-680.

Kaznov, V. and Seeman, M. 2010. "Outdoor navigation with a spherical amphibious robot." In *Proceedings of Intelligent Robots and Systems* (Taipei, Oct. 2010). 5113-5118.

Kim, J.; Kwon, H. and Lee, J. 2009. "A rolling robot: Design and implementation." In *Proceedings of 7th Asian Control Conference* (Hong Kong, Aug. 2009). 1474-1479.

Krieger, K. 2013. "Meet GuardBot!." *Physics Today Online*, Aug. 2013, http://dx.doi.org/10.1063/PT.4.2536

Laplante, J.; Masson, P. and Michaud, F., 2007. *Analytical Longitudinal and Lateral Models of a Spherical Rolling Robot.* [online]. Available at: http://introlab.3it.usherbrooke.ca/papers/TRRoball.pdf (Accessed 10.5.2013).

Li, Z. and Canny, J. 1990. "Motion of two rigid bodies with rolling constraint." *IEEE Transactions on Robotics and Automation* 6, No.1, 62-72.

Liu, D. and Sun, H. 2010. "Nonlinear sliding-mode control for motion of a spherical robot." In *Proceedings of 29th Chinese Control Conference* (Beijing, 29–31 July). 3244-3249.

Liu, D.; Sun, H. and Jia, Q. 2008. "Stabilization and path following of a spherical robot." In *Proceedings of IEEE International Conference on Robotics, Automation and Mechatronics* (Chengdu, Sept. 2008). 676-682.

Mahboubi, S.; Seyyed Fakhrabadi, M.M. and Ghanbari, A. 2013. "Design and implementation of a novel spherical mobile robot." *Journal of Intelligent and Robotic Systems: Theory and Applications* 71, No.1, 43-64.

Michaud, F. and Caron, S. 2002. "Roball, the rolling robot." *Autonomous Robots* 12, No.2, 211-222.

Montana, D.J. 1988. "Kinematics of contact and grasp." *International Journal of Robotics Research* 7, No.3, 17-32.

Morinaga, A.; Svinin, M. and Yamamoto, M. 2012. "On the motion planning problem for a spherical rolling robot driven by two rotors." In *Proceedings of IEEE/SICE International Symposium on System Integration* (Fukuoka, Dec. 2012). IEEE, 704-709.

Mukherjee, R.; Minor, M.A. and Pukrushpan, J.T. 1999. "Simple motion planning strategies for spherobot: a spherical mobile robot." In *Proceedings of the 38th IEEE Conference on Decision and Control* (AZ, 1999). 2132-2137.

Mukherjee, R.; Minor, M.A. and Pukrushpan, J.T. 2002. "Motion planning for a spherical mobile robot: Revisiting the classical ball-plate problem." *ASME Journal of Dynamic Systems, Measurement, and Control* 124, No.4, 502-511.

Nagai, M. 2008. *Control System of a Ball-shaped Robot.* Master's Thesis, Department of Automation and Systems Technology, Helsinki University of Technology.

Nandy, G.C. and Xu, Y. 1998. "Dynamic model of a gyroscopic wheel." In *Proceedings of IEEE International Conference on Robotics and Automation* (Leuven, May 1998). IEEE, 2683-2688.

Otani, T.; Urakubo, T.; Maekawa, S.; Tamaki, H. and Tada, Y. 2006. "Position and attitude control of a spherical rolling robot equipped with a gyro." In *Proceedings of IEEE International Workshop on Advanced Motion Control* (Istanbul, March 27-29). IEEE, 416-421.

Sang, S.; Shen, D.; Zhao, J.; Xia, W. and An, Q. 2011. "Prototype Design and Motion Analysis of a Spherical Robot." *Communications in Computer and Information Science* 134, No.1, 284-289.

Sang, S.; Zhao, J.; Wu, H.; Chen, S. and An, Q. 2010. "Modeling and simulation of a spherical mobile robot." *Computer Science and Information Systems* 7, No.1, 51-62.

Sang, S.J.; Shen, D.; Zhao, J.C.; Hu, J.Y. and An, Q. 2011. "Analysis and Simulation of a Spherical Robot." *Advanced Materials Research* 171 - 172, 748-751.

Spitzmüller, S. 1998. *Microcontroller based control system for a rolling minirobot.* Master's Thesis, Department of Automation and Systems Technology, Helsinki University of Technology.

Svinin, M. and Hosoe, S. 2006. "Simple motion planning algorithms for ball-plate systems with limited contact area." In *Proceedings of IEEE International Conference on Robotics and Automation* (Orlando, FL, May 2006). IEEE, 1755-1761.

Svinin, M. and Hosoe, S. 2008. "Motion Planning Algorithms for a Rolling Sphere With Limited Contact Area." *IEEE Transactions on Robotics* 24, No.3, 612-625.

Svinin, M.; Morinaga, A. and Yamamoto, M. 2012a. "An analysis of the motion planning problem for a spherical rolling robot driven by internal rotors." In *Proceedings of IEEE International Conference on Intelligent Robots and Systems* (Vilamoura, Oct. 2012). IEEE, 414-419.

Svinin, M.; Morinaga, A. and Yamamoto, M. 2012b. "On the dynamic model and motion planning for a class of spherical rolling robots." In *Proceedings of IEEE International Conference on Robotics and Automation* (Saint Paul, May 2012). 3226-3231.

Xu, Y.; Au, K.W.; Nandy, G.C. and Brown, H.B. 1998. "Analysis of actuation and dynamic balancing for a single-wheel robot." In *Proceedings of IEEE/RSJ International Conference on Intelligent Robots and Systems* (Victoria, BC, Oct. 1998). IEEE, 1789-1794.

Ylikorpi, T. and Suomela, J. 2007. "Ball-shaped Robots." In *Climbing & Walking Robots, Towards New Applications,* Z. Houxiang Zhang (Ed.). InTech, Vienna, 235-256.

Zhan, Q.; Cai, Y. and Yan, C. 2011. "Design, analysis and experiments of an omni-directional spherical robot." In *Proceedings of IEEE International Conference on Robotics and Automation* (Shanghai, May 2011). IEEE, 4921-4926.

Zheng, M.; Zhan, Q.; Liu, J. and Cai, Y. 2011. "Control of a Spherical Robot: Path Following Based on Nonholonomic Kinematics and Dynamics." *Chinese Journal of Aeronautics* 24, No.3, 337-345.

AUTHOR BIOGRAPHIES

TOMI YLIKORPI went to Helsinki University of Technology and obtained his Master's degree in 1994 in Mechanical Engineering. He obtained his Licentiate's degree in Automation Technology in 2008 and currently works at Aalto University with design and modelling of mechanical systems. His e-mail address is: TOMI.YLIKORPI@AALTO.FI

PEKKA FORSMAN received his PhD in Automation technology from Helsinki University of Technology in 2001. He is currently university lecturer at Aalto University. His research interests include field and service robotics, human-robot interfaces as well as localization and navigation methods. His e-mail address is: PEKKA.FORSMAN@AALTO.FI

AARNE HALME started his career in 1966 at Helsinki University of Technology. From 1985 until lately he has been the Professor and Head of the Automation Technology Laboratory at Helsinki University of Technology. He is one of the very first pioneers in development and analysis of ball-shaped rolling robots. His e-mail address is: AARNE.HALME@AALTO.FI